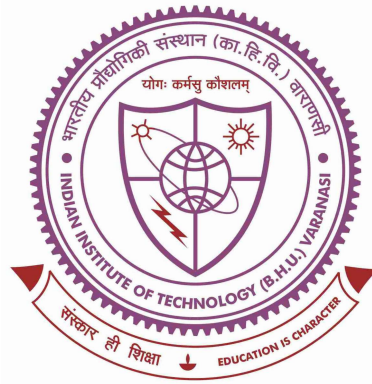


Study of Structure and Dynamics of the InterStellar Medium in Nearby Spiral Galaxies



Thesis submitted in partial fulfillment

for the Award of Degree

DOCTOR OF PHILOSOPHY

by

MEERA NANDAKUMAR

DEPARTMENT OF PHYSICS

INDIAN INSTITUTE OF TECHNOLOGY

(BANARAS HINDU UNIVERSITY)

VARANASI - 221005

ROLL NUMBER

17171018

YEAR OF SUBMISSION

2022

To my loved ones . . .

Certificate

It is certified that the work contained in the thesis titled **Study of Structure and Dynamics of the InterStellar Medium in Nearby Spiral Galaxies** by **Mrs Meera Nandakumar**, Roll Number **17171018**, has been carried out under my supervision and that this work has not been submitted elsewhere for a degree.

It is further certified that the student has fulfilled all the requirements of Comprehensive Examination, Candidacy and SOTA for the award of **Ph. D. Degree**.

Date

Supervisor

Place

Dr. Prasun Dutta
Assistant Professor
Department of Physics
IIT (BHU), Varanasi

Declaration

I, **Meera Nandakumar**, certify that the work embodied in this thesis is my own bona-fide work and carried out by me under the supervision of **Dr Prasun Dutta** from 26/07/2017 to 20/06/2022 at the **Department of Physics**, Indian Institute of Technology (BHU), Varanasi. The matter embodied in this thesis has not been submitted for the award of any other degree/diploma. I declare that I have faithfully acknowledged and given credits to the research workers whenever and wherever their works have been cited in my work in this thesis. I further declare that I have not wilfully copied any others' work, paragraphs, text, data, results, etc., reported in journals, books, magazines, reports dissertations, theses, etc., or available at websites and have not included them in this thesis and have not cited as my own work.

Date

Signature of Student

Place

Meera Nandakumar

Certificate by the Supervisor

It is certified that the above statement made by the student is correct to the best of my knowledge.

Supervisor

Head of Department

Dr. Prasun Dutta

Copyright Transfer Certificate

Title of the Thesis: **Study of Structure and Dynamics of the InterStellar Medium in Nearby Spiral Galaxies**

Name of the Student : **Meera Nandakumar**

Copyright Transfer

The undersigned hereby assigns to the Indian Institute of Technology (Banaras Hindu University) Varanasi all rights under copyright that may exist in and for the above thesis submitted for the award of the *Doctor of Philosophy*.

Date:

Signature of the Student

Place:

Meera Nandakumar

Note: However, the author may reproduce or authorize others to reproduce material extracted verbatim from the thesis or derivative of the thesis for author's personal use provided that the source and the Institute's copyright notice are indicated.

Acknowledgements

After a couple of sleepless nights and stressful months, I think this is the time where I need to sit and have some rewind to my life so far. I believe this could be the best chance where I can remember a few persons that have influenced me in this short life.

If I go back to my childhood, I used to spend my entire time with my grandparents Late. Mr Gopinathan and Mrs Hymavathiamma. I always remember the precious moments that I spent with them during my childhood. Though as a mischievous kid I used to always eat their head off, I can understand now how much they enjoyed it then. I was lucky to be their only grandchild until my seventh age and I really enjoyed that privilege. I remember my maternal grandfather Late Mr Pankajakshakurup, who was my first childhood friend or pal whom with I played a lot, unfortunately for a small period. My grandmother Late Mrs Ponnama used to advise me a lot telling 'Don't do this' or 'Do this'. Though I don't like them at all as a child, I can understand her feeling of care towards me that drives her to say those. I always miss those nice times which I spent with my two grandmothers, hearing their childhood stories.

The void which I used to feel from not having a sibling for the first seven years of my life, was compensated by a few people who are close to my heart. Apart from my grandparents, one major person that made those days sweet and precious is my maternal uncle Mr Balachandran. My main motivation for visiting my mother's home is that I can meet my uncle and play with him. He used to take me to a lot of places in his RX tiger bike where me sitting on top of it and I literally feels like a King while riding. Another person that whom I always like to chat with is my paternal Aunt, Mrs Rekha. I remember the day when she came to our family as a new bride where I felt initially complete strangeness toward her. But now, I am amazed by the transformation that she created in me so that rather than my Uncle Mr Balakrishnan, I feel close to her.

In my third standard, I get a treasure which I was really wanting for so many years, my sister Meenu Nandakumar. I remember the moment I saw her for the first time, literally she looks like a mouse. I always want to spend time with her. Shortly I got two more gifts, Krishnedhu and Devanarayan. I enjoyed the fights that I intentionally made with three of them for zero reasons. I really wish I could have reduced my age few years so that I can be a part of their group and play with them. I regret missing many of the precious moments and the playtime with them that I lost for useless reasons.

As I don't have many friends in my childhood or I was not good at maintaining a friendship, I have very few friends from my college IISER, Bhopal like Jinu, Archana, Muthu and Shibu. I remember the days I spent in Muthu's home in Mysore, where I used to complete many of my deadlines during my PhD. I really enjoyed those days. I would like to thank a few people in NCRA, Pune where I spent quite a time. I started my journey in Radio Astronomy there by doing a project with Dr Niruj Ramanujam and later a one-year project with Dr Jayaram Chengalur. Those experiences are truly worthy and critical so that, often many problems in this thesis have been easily solved out because of the basic knowledge that I have gained from there. I would like to give special mention to a few friends in NCRA, Barnali, Sushama, Suraj, Apurba, Nissim, Nayana and Binny. Suma Murthy, my dear labmate and roommate during my NCRA days, I always miss the time I spent with her. I would like to thank people in GMRT, Pune for helping me during the observations.

The result of the work that I have done for the last two years of my PhD would not become real without the support of the pillar of Vidyalam family, Mrs Omana (my Omanakutty). I am privileged to have been the daughter of my parents by karma, Mr Vijayan V K and Mrs Omana. Their support and care are priceless and nothing can be replaced them. I would say, I want to be like Omanakutty while supporting and caring for my family. My sister Vidya, I enjoyed the time that she used to have in our home.

Thanks, Chechi for caring for me and supporting me. Finally, my little King, my Manav, my nephew no words can express what I feel about him. He is the only person, from which I always wanted to hear calling me 'Meera'.

My guide Dr Prasun Dutta, when I met him eight years back in IISER, I didn't realise then that this person was going to be a part of my life. He is one of the people to whom I would like to dedicate this thesis. I know he really wanted this.

I should mention my fellow labmates, Pavan, Jais, and Urvashi and the good moments that I spent with them. I remember the conference days and workshop days that we spent together. Also, I would like to give a special mention to Kanchan, who supported and helped me for many clerical works.

I would like to acknowledge here the cluster facility of VLA, New Mexico, where I could do the data reduction part of one of my data during the covid lockdown. Also, I remember the significant role played by the computers AKASH, ORION, ISM, HELIOUS and my own laptops, in carrying out the various computational work during my PhD days. I would like to thank the DST-INSPIRE fellowship for funding this work. I would like to acknowledge the entire faculty and other staff of the Department of Physics of IIT(BHU), Varanasi for supporting me several times in the last five years.

Finally, I will stop here by mentioning the pillars of my life to whom I am always indebted; my parents who made me as Meera, Mr Nandakumar P G and Mrs Geetha P and my existence Mr Vipin V.

Meera Nandakumar

D/o Nandakumar P G

Abstract

Spiral galaxies are composed of stars and interstellar medium (ISM) residing in a dark matter halo. They are very much dynamically active and are the playgrounds for the ISM to give birth to stars. The large scale distribution in dark matter halo, differential galactic rotation, interaction with satellite galaxies, star formation and its feedback, all give rise to isotropic and anisotropic density and velocity structures in the ISM. The interstellar medium acts as a compressible fluid with turbulent flows that later give rise to scale invariant density and velocity structures. The density structures give rise to fragmentation in the gas helping it to collapse. On the other hand, the turbulent dynamics raise the pressure and at small clumps, collapses are lengthened. Such scale invariant structures in both velocity and density have been seen observationally in our Galaxy and its satellites at scales of the order of a few astronomical units to a few hundreds of parsec (Crovisier and Dickey, 1983; Green, 1993). Recent observations in nearby spiral galaxies have established the existence of scale invariant coherent density structures at the scales of a few kiloparsecs, almost at the scale of the galactic discs (Dutta et al., 2013). The observed structures in our galaxy at scales of a few hundreds of parsec and lower are attributed to compressible fluid turbulence generated by the supernovae feedback. However, related dynamics and the generation mechanism of the large scale structures probed recently in external spiral galaxies are now well established. In this thesis, we design and implement various statistical estimators and use them to investigate the large scale structure and dynamics of the ISM in these spiral galaxies. We comment on the driving mechanism behind the large scale structures based on our observations and access their relation to star formation.

We use radio interferometric observation of H I 21-cm emission line as a tracer of the ISM. Radio interferometers measure visibility function, roughly the Fourier transform of

the sky brightness distribution. The visibilities are measured only at discrete points in the baseline plane, the Fourier conjugate to the angular separation in the sky. To probe the structure and dynamics of the ISM, we need to estimate the large scale dynamics and morphology of the gas. The imprint of turbulence can be traced through the two-point statistics of the density and velocity, like their spatial power spectrum. The limited measurements of visibility create challenges to estimate various statistics of the density and velocity unbiasedly. In this thesis, we first use simulation of radio interferometric observations of external spiral galaxies to investigate the efficacy of estimation of the column density distribution from the reconstructed images from visibilities. We also compare the image based and visibility based column density power spectrum estimators to assess their relative merits in this context. We find that the Natural weighting scheme in the CLEAN deconvolution algorithm unbiasedly estimates the large scale distribution of the H I, whereas to estimate the power spectrum direct use of visibilities gives an unbiased result.

Turbulence is a stochastic random process which creates scale invariant structures in density and velocity that can be quantified through the spatial power spectrum measurements of density and velocity. The power spectrum of turbulence generated structures follows a power law, with its slope indicating the nature of turbulence. Combined knowledge of density and velocity power spectrum lets us infer the energy supply and driving mechanism. Following the idea of Dutta (2016) we develop and implement Visibility Moment power spectrum Estimators (VME) of H I column density and line of sight velocity power spectrum directly from the observed visibilities. We measured the column density and the line of sight velocity power spectrum of spiral galaxies NGC 5236 and NGC 6946. We present here the evidence of large scale energy cascade in these galaxies observed in more than one decade of length scales between ~ 100 parsecs to 15 kiloparsecs. We find that the compressive forcing is responsible to drive the turbulence cascade at the scales of

kiloparsec and higher in NGC 5236. While a combination of solenoidal and compressive force acts a generating mechanism for the turbulence in NGC 6946. The cascade brings down energies to the scales of 100 pc which is comparable to the energies injected by supernovae feedback.

We review the instability of a star-forming disc in presence of turbulence (Leroy et al., 2008). The instabilities are assessed through modified Toomre criteria of two fluid disc models incorporating effects of turbulent generated log-normal H I density distribution. We choose a sample of three galaxies, NGC 4736, NGC 3351 and NGC 5236 with similar stellar and gas mass and velocity dispersions but different disc scale length and star formation rates per unit area. We find that the H I is unstable at scales greater than a few kiloparsecs in the regions with high H I column density, at smaller scales the correlation between high H I column density and instability dies down indicating conversion of H I to the molecular cloud. At small scales, we also see more fragmented regions of instabilities commensurate with the high star-forming regions. We observe that for NGC 3351, even at small scales the high ISM column density regions do not form stars effectively. Comparing the column density power spectrum slopes in these three galaxies we conclude that turbulent fragmentation has a significant role in inducing instabilities which eventually seed the star formation.

Several dynamical effects like interaction with satellite galaxies, accretion of the intergalactic medium, tidal effects etc create bending waves in the galactic discs. Observationally these are traced as corrugation in edge-on discs for density and in the face on stellar disc for velocity mostly in optical or infrared (Narayan et al., 2020; Sánchez-Gil et al., 2015). In this thesis, we investigate the corrugation in gas density and velocity using 21-cm observations of the galactic discs. With a sample of six nearby spiral galaxies, we estimate the multipole moments of the column density and line of sight velocity corrugation. We see all these galaxies are vertically perturbed indicating that corrugations or bending is a

common phenomenon. We also see that $m = 2$ is the dominant mode that forms around 50% of the identified modes in both density and velocity space. This probably suggests that $m = 2$ mode may be long-lived than the higher modes. Most of the anisotropies are also found near the $0.6R_{25}$ of the corresponding galaxies suggesting the likely cause of these structures is the gravitational interaction of the gas with the stellar disc.

This thesis establishes the origin and role of large scale turbulence cascade in the disc galaxies and explores vertical corrugations in the spiral galaxies. Some of the results presented here had indications in recent simulations of the discs, others need further theoretical study.

List of Symbols

Acronyms

Acronym	Full form
H I	Neutral hydrogen
H II	Ionized hydrogen
CO	Carbon Monoxide
PA	Position Angle
ISM	Interstellar Medium
SFR	Star Formation Rate
NGC	New General Catalogue
DDO	David Dunlap Observation
SMC	Small Magellanic Cloud
LMC	Large Magellanic Cloud
AIPS	Astrophysical Image Processing System
CASA	Common Astronomy Software Application
VLA	Very Large Array
GMRT	Giant Metrewave Radio Telescope
SKA	Square Kilometer Array
THINGS	The H I Nearby Galaxy Survey

Symbols

Symbols	Definitions
H_2	Molecular hydrogen
\vec{U}	Baseline in wavelength
ν	Observing frequency in Hz
$\vec{\theta}$	Angle in the sky measured from the centre of the galaxy
$V(\vec{U}, \nu)$ or $V(\vec{U})$	Visibility
$V_j(\vec{U})$	j^{th} moment of Visibility
$I(\vec{\theta}, \nu)$	Specific Intensity
$M_j(\vec{\theta})$	j^{th} moment of specific intensity
\bar{I}_ν	Smooth part of $I(\vec{\theta}, \nu)$
$\delta I(\vec{\theta}, \nu)$	Fluctuating part of $I(\vec{\theta}, \nu)$
$W(\vec{\theta})$	Window function
$A(\vec{\theta})$	Antenna primary beam
$\mathcal{N}(\vec{U})$	Noise at baseline \vec{U}
$I_C(\vec{\theta})$	Reconstructed image from measured visibilities
$P_{\text{HI}}(\vec{U})$	H I column density Power spectrum
$P_C(\vec{U})$	Image Based density Power spectrum
$P_V(\vec{U})$	Visibility based density Power spectrum
$P_v(\vec{U})$	H I line of sight velocity Power spectrum
$1M_\odot$	Solar mass: $1M_\odot = 1.99 \times 10^{30}$ kg

Symbols	Definitions
U_{min}	Minimum value of the baseline above which power spectrum is a power law
U_{max}	Maximum value of the baseline below which power spectrum is a power law
R_{min}	Minimum length-scale above which power spectrum is a power law
R_{max}	Maximum length-scale below which power spectrum is a power law
A	Amplitude of the power law
α	Power law index
c	Speed of light = 299792458 m/s
ν_0	Emission frequency of H I 21 cm line = 1420.40575 MHz
h_z	Scale height of the galaxy
i_{HI} or i	H I inclination angle
ω	Axisymmetric frequency of perturbation waves
κ	Epicyclic frequency
R	Galacto-centric radius
Q	Toomre Parameter
k	Wavenumber
Σ	Surface density
M	Mach Number
1pc	1 parsec = 3.08×10^{16} m

Symbols	Definitions
\mathcal{R}	Ratio of the total intensity to the standard deviation of intensity fluctuations
R_{25}	Optical extent at which B band surface brightness is at the level of 25 magnitude arcsec ⁻²
G	Gravitational Constant, $6.6743 \times 10^{-11} \text{ m}^3 \text{ kg}^{-1} \text{ s}^{-2}$
m	azimuthal bending mode
\AA	unit of length, $1\text{\AA} = 10^{-10} \text{ m}$

Table of contents

Acknowledgement	xiv
Abstract	xix
List of Symbols	xxiii
List of figures	xxvii
List of tables	xxxv
1 Introduction	1
1.1 Different traces of galaxy elements	3
1.2 Interstellar medium at large scales	5
1.2.1 ISM Turbulence	5
1.2.2 Anisotropy in ISM	7
1.3 Interaction between ISM and star formation	9
1.4 Motivation	10
2 Probing large scale turbulence	15
2.1 H I as a probe for structure and dynamics	15
2.2 Radio Interferometric observation	18
2.3 Two point correlation statistics	22

2.3.1	Autocorrelation function and Structure function	22
2.3.2	Power spectrum	23
2.4	Efficacy of reconstructed image	25
2.4.1	Simulating model visibility dataset	25
2.4.2	Simulated visibility data	31
2.4.3	One Point statistics: large-scale distribution of specific intensity	33
2.4.4	Power Spectrum estimators	34
2.4.5	Analysis and Results	37
2.5	Visibility moment estimators	49
2.5.1	Visibility moments	50
2.5.2	Power spectrum of column density and velocity	51
2.6	Summary	53
3	Energy cascade in external disc	55
3.1	Sample selection	55
3.2	Observations and data analysis	58
3.2.1	NGC 5236	58
3.2.2	NGC 6946	59
3.2.3	Combining with the THINGS data	60
3.3	Implementation of the visibility moment estimator	60
3.4	Results	63
3.5	Discussion	69
3.5.1	Compressive turbulence in NGC 5236	73
3.5.2	Nature of turbulence in NGC 6946	76
3.6	Summary	78
4	Instability and star formation in the Interstellar Medium	79

4.1	Instability in two fluid disc	80
4.2	Sample selection and observations	83
4.3	Estimation of two-fluid Toomre parameter	87
4.4	Results and Inferences	91
4.4.1	Correlation with H I	92
4.4.2	Correlation with H ₂ , Σ_* , SFR	98
4.4.3	Role of turbulence	99
4.5	Summary and Conclusions	103
5	Anisotropic modes in spiral galaxies	105
5.1	Anisotropy and bending waves	105
5.2	Quantifying anisotropies using harmonic decomposition	108
5.3	Sample selection	113
5.4	Anisotropic signature for the galaxy NGC 3621	114
5.5	Results for entire sample	118
5.5.1	Identifying anisotropic modes	122
5.6	Summary	129
6	Conclusions and Summary	131
	References	137

List of figures

2.1	Greyscale image showing the natural weighted moment zero map of the galaxy NGC 628. Contours represent the model window function based on this map (see eqn (2.15)). Note that the range of values in the pixels of these maps differ. We have scaled the pixel values to keep the maximum pixel value as unity for both the maps.	28
2.2	Power spectrum for the first term $W(\vec{\theta})\bar{I}$ in eqn. (2.13) (solid black line) is compared with the power spectrum of $I(\vec{\theta})$ for the model image (blue dashed line) with $\mathcal{R} = 5$ and $\alpha = -1.5$. Observe that for $U > 1 k\lambda$ there is a significant deviation between the two. The green dot-dash line corresponds to a power law with index -1.5 . Clearly, the power spectra of $I(\vec{\theta})$ follow a power law for $U > 1 k\lambda$ and has the slope of -1.5	30
2.3	Figure showing the sampling function for the simulated observation presented here. Black points are the places in the baseline plane where the visibilities are measured.	31
2.4	Figure showing the power spectrum of the dirty beam for the uniform, robust and natural weighted beams for the sampling function given in Figure 2.3.	32

-
- 2.5 Window functions of the reconstructed images using different weighting schemes are shown in contours against the grey scale plot of the window function of the model image corresponding to $\mathcal{R} = 5$, $\alpha = -1.5$. The scales of the contours are relative here. 38
- 2.6 This figure compares the azimuthally averaged window functions estimated using different weighting schemes with that of the input image. The colour bands for each estimate represents the error. 38
- 2.7 Comparison of the azimuthally averaged window functions estimated from the input model (black solid line) and the reconstructed natural weighted image (red triangles) are shown for all six simulations. 41
- 2.8 This figure compares the power spectrum estimated using the visibility based estimator and the image based estimator for all three different weighting schemes against the model power spectrum. The shaded area corresponds to the error associated with each estimate. 43
- 2.9 Comparison of the power spectrum estimated from the input model (black solid line), using the visibility based estimator (grey pentagons) and image based estimators from the uniform weighted image (blue circles) are shown for all six simulations. The amplitudes of the y-axes for different panels are scaled arbitrarily to keep the power spectra in the same range in all plots. 44
- 2.10 The image and visibility based estimates of α are compared for different simulations and weighting schemes. In each panel, we plot the image based estimate α_I against the visibility based estimate α_V for all six simulations. The dashed line corresponds to an exact match. The meaning of different markers is given in the left most panel. Three panels in this figure correspond to three different weighting schemes, with a left to right giving uniform, robust and natural weightings respectively. 46

- 2.11 The Figure shows the power spectra calculated from the residual images after the point source subtraction for the point sources influencing 1%, 10% and 30% of the field of view. 47
- 3.1 The SDSS optical (blue-band) images of the two galaxies are shown in background grey scale. The H I column density maps from THINGS survey are plotted with black contours. The contour levels are at $(1, 5, 10, 15, 20) \times 10^{20}$ atoms cm^{-2} for both the galaxies. Optical images are obtained from the public domain of Skyview survey metadata (Lasker et al., 1990). The x-axis is the right ascension given in hh:mm:ss (hour, minute, second) and the y-axis is declination given in dd:mm:ss (degree, arc minute, arc second). 61
- 3.2 Column density power spectrum of NGC 5236(top) and NGC 6946(bottom) as a function of baseline. The corresponding length scales are also shown in the top margin. The black solid circles correspond to the measurement of the column density from the THINGS data alone. The black open circles correspond to measurement using only the uGMRT/eVLA observations. These two sets of points are scaled down by a factor of ten for display purpose. The black solid squares with error bars give the power spectra measurements combining the old THINGS and the new observations. A best fit power law to the combined measurement is shown using black solid lines. 65
- 3.3 The turbulent velocity power spectrum of NGC 5236(top) and NGC 6946(bottom) as a function of baseline. The corresponding length scales are also shown in the top margin. The black solid circles with error bars correspond to the measurement from the uGMRT observations in NGC 5236 and combined observations for NGC 6946. A best fit power law to the combined measurement is shown using black solid lines. 68

-
- 3.4 Median velocity dispersion is plotted with galacto-centric radius (circles) for NGC 5236 and NGC 6946. The vertical line corresponds to the respective R_{25} of the galaxy. The horizontal line corresponds to the turbulence velocity dispersion at 6 kpc scale for both the galaxies. 75
- 4.1 Left column shows the H I surface density maps of three galaxies after grid matching. The Middle column is H_2 surface density and the right column is star mass density maps. 88
- 4.2 Each row in the Left column shows the two fluid Toomre parameter Q_T estimated in entire region in three galaxies for different wavelength scales. Each row in the right column shows galactic center only in enlarged view for the respective plots. 90
- 4.3 Left panel of figure 4.3 shows the distribution of pixels in $Q_T - \Sigma_{HI}$ plane in a density plot giving the number of pixels in a given range. Right hand side of figure 4.3 shows the Σ_{HI} with overplot of Q_T values equals to 2,1,0.6 as red, black, white contours respectively. The values are noted at the top of the panel. 92
- 4.4 Figure (a) is the Spearman correlation coefficient of Q_T and Σ_{HI} are plotted as function of λ in parsec for NGC 5236. Figure (b) shows the separate probability density of Q_T values at $\lambda \sim 1$ kpc inside (black) and outside (red) the stellar disc. Blue shaded region shows the $Q_T < 1$ region. Histogram plot show in the inset is that of Σ_{HI} with legend follows the same order. 93

4.5 The correlation coefficient between Q_T and different surface densities are plotted as a function of λ in parsec for all three galaxies. First row shows the correlation between Q_T and H I from inside and outside the stellar disc. Second row shows that between Q_T and surface density of H_2 , stellar mass and SFR in blue, green and red lines respectively. 95

4.6 The spearman correlation coefficient between σ_{HI} and Q_T , Σ_{SFR} , Σ_{HI} plotted as function of λ in parsec for three galaxies are plotted in left pannel. Red lines with star points show the correlation coefficients between σ_{HI} and Σ_{HI} , black lines with square markers show that of σ_{HI} and Σ_{SFR} , blue lines with triangle markers show the same for σ_{HI} and Q_T . In right pannel, correlation coefficients between σ_{HI} and Σ_{H_2} , Σ_* are plotted. Green lines with square makers show the correlation with Σ_{H_2} and the purple lines with circle show the case for Σ_* . First row shows the plots for NGC 5236, second row is for NGC 4736 and third one is for NGC 3351. 101

5.1 A toy model showing bending waves in a sheet leading to column density and velocity corrugations. The top panel show the cross section of a corrugated disc with the V_{rot} showing that the gas velocity follow the bending. The middle and bottom panel show the resulting column density and line of sight velocity oscillations (for $V_{rot} = 220 \text{ km s}^{-1}$) for two inclination angles of 0° (black) and 20° (blue). 107

- 5.2 The top panel shows the function $f_1(R, \phi)$ for $R = 12$ kpc (blue dots) for the galaxy NGC 3621. Five-sigma uncertainties are also plotted for the same as error bars. The black continuous line represents the first two moments of this function. In the bottom panel we show the column density, line of sight velocity and velocity fluctuations $\delta N_{\text{HI}}(R, \phi)$, $\delta v(R, \phi)$ and $\delta \sigma_v(R, \phi)$ with ϕ at the same radius R . The shaded regions represents one-sigma uncertainties. The y-axis on the left side shows the scale for $\delta N_{\text{HI}}(R, \phi)$ and the y-axis on right side shows the scale for $\delta v(R, \phi)$ and $\delta \sigma_v(R, \phi)$. Note that the mean values of these quantities are different at different radius. 116
- 5.3 The figure shows the fluctuations in column density ($\delta N_{\text{HI}}(R, \phi)$), line of sight velocity ($\delta v(R, \phi)$) and velocity dispersions ($\delta \sigma_v(R, \phi)$) for the galaxy NGC 3621 projected in the galactic plane. White circle represents the optical extent with radius $\sim R_{25}$ 117
- 5.4 The three columns show the Spearman rank correlation coefficients (black dots) estimated for the respective pairs of residual maps for NGC 3621. Shaded region indicates chance correlation. The figures share same y-axis giving the radius R . The horizontal black line represents R_{25} of the galaxy. 117
- 5.5 Amplitudes of modes in residual maps of column density (left) and los velocity (right) are shown for different radii R . The white horizontal line corresponds to the R_{25} indicating the optical disc of the galaxy. 118
- 5.6 Figure shows the fluctuations in column density (δN_{HI}), line of sight velocity (δv) and velocity dispersions ($\delta \sigma_v$) for all the six galaxies in our sample. White circle represents the optical extent of the respective galaxy with a radius $\sim R_{25}$ 119

5.7 The Spearman rank correlation coefficients for all three pairs of $\delta N_{\text{HI}}(R, \phi)$, $\delta v(R, \phi)$ and $\delta \sigma_v(R, \phi)$ as a function of radii for all the galaxies in our sample. The shaded regions corresponds to chance correlation. The horizontal lines denote R_{25} for those galaxies. 120

5.8 The multipole amplitudes for residual maps of column density (left) and los velocity (right) at different radii for all galaxies in our sample. The horizontal lines denote R_{25} for those galaxies. 123

5.9 First few multipole amplitudes A_{m0} (left) and A_{m1} (right) at different radius for all galaxies in our sample. The vertical lines denote R_{25} for those galaxies. 124

5.10 Column density (left) and line of sight velocity (right) mode peaks shown for all galaxies. The vertical axes show their maximum amplitude and the horizontal axes show the radial positions in their host galaxies. For the ease of comparision, radial positions are normalized by R_{25} of respective galaxies. In the top panel, the amplitude of all modes for different galaxies (color coded) are shown. The bottom panel shows the same color coded mode-wise. Note that we do not include $m = 1$ velocity mode here. . . . 126

5.11 Various statistics related to the column density (left) and velocity modes (right) are shown. Top panels show the number of detected density and velocity peaks for $m = 2, 3 \& 4$ (solid colors) alongside with their average amplitudes (bars with stars) considering all galaxies. The bottom panel shows a histogram of radial position of these modes. 127

List of tables

2.1 Table summarising the result of comparison between different estimates of the window function and power spectrum. Efficacy to reproduce the model window function from an estimated image is quantified by χ (see eqn (2.25)). We tabulate the values of α_V and α_I for each model to assess the merit of different estimators in the table. The headers ‘U’, ‘R’ and ‘N’ correspond to the uniform, robust and natural weighting schemes respectively. 42

3.1 Some parameters of the selected galaxies. Columns 1-9 gives 1) Name of the galaxy, 2) Distance to the galaxy in Mpc, 3) Average H I inclination angle, 4) Position angle, 5) Optical radius R_{25} in kpc, 6) H I extent in kpc which is major and minor axis at the level of column density brightness of 10^{19} atoms cm^{-2} , 7) Star Formation Rate, 8) H I mass, 9) Dynamical Mass. These values are obtained from the following references: Bottinelli and Gouguenheim (1973); de Blok et al. (2008); Ianjamasimanana et al. (2015); Leroy et al. (2008); Pierce (1994); Radburn-Smith et al. (2011); Schmidt et al. (1992); Walter et al. (2008) 56

3.2 Different parameters regarding the H I observations of two galaxies is given in this table. Galaxy name, Telescope used for observation, date of observation, bandwidth and channel number, total integration time on source are given in each column. 58

-
- 3.3 Result of power law fit ($P = AU^\alpha$) to the column density (P_{HI}) and velocity (P_v) power spectra. The power law amplitude (A) at one steradian, best fit slope α , $1 - \sigma$ errors associated with the fit, the reduced χ^2 values and the range of fit in baselines and corresponding length scale ranges are shown. The density power spectra fit is shown for the THINGS data, the new observation data and the combined power spectra. The velocity power spectra results are only from the GMRT data for NGC 5236 and from combined data for NGC 6946. The amplitudes for the density spectra are scaled by a factor of 10^4 and have a unit of steradian. *The amplitude of the velocity spectra is not scaled and is given in $(\text{km sec}^{-1})^2$ steradian. 66
- 3.4 Power spectral slope for density and velocity for different theoretical models of turbulence and simulations. All the spectral slopes are given for what is expected for turbulence in the thin disk as the case for this observational result. Here α is the compressibility factor. 70
- 4.1 Following details of the three galaxies are given here; Morphology type, Distance, position angle, inclination, optical size(R_{25}), R_{HI} radius corresponding to semi major axis extent at a H I column density of 10^{19} atoms cm^{-2} , total H I mass from integrating values within the H I extent, total stellar mass and total molecular mass from integrating values within in $1.5R_{25}$ and star formation rate. References as follows: (1) Walter et al. (2008), (2) de Blok et al. (2008), (3) Bottinelli and Gougenheim (1973), (4) Leroy et al. (2008), (5) Ann et al. (2015) and (6) Crowther (2013) . . . 84

- 4.2 Table giving observation details of the three galaxies. H I maps are from THINGS, H₂ maps are derived from CO maps of the Nobeyama survey and the BIMA survey. The star mass maps are obtained from WISE survey and both have the same resolution parameters. References as follow (1) Walter et al. (2008), (2) Jarrett et al. (2013), (3) Kuno et al. (2007), (4) Helfer et al. (2003). 86
- 4.3 Table shows different quantities indicating star formation and turbulence in three galaxies. Column(1) - Galaxy name, Column(2) - total H I mass, Column(3) - star formation rate per unit area, Column(4) - slope of H I column density power spectrum, Column(5) - range of length scale where power law power spectrum is measured, Column(6) - mean H I velocity dispersion. 103
- 5.1 Table giving different properties of the six galaxies. Column 1: galaxy name; Column 2: distance (D), Column 3: average inclination angle (*i*); Column 4: average position angle (PA); Column 5: velocity resolution of THINGS data cube; Column 6: H I extent (R_{HI}) at a H I column density of 10^{19} atoms cm⁻², Column 7: optical extent (R_{25}), Column 8: References : (1) de Blok et al. (2008), (2) Walter et al. (2008), (3) Freedman et al. (2001), (4) Karachentsev et al. (2004), (5) Drozdovsky and Karachentsev (2000), (6) From LEDA survey (Prugniel et al., 2001), (7) Dutta et al. (2013). 114
- 5.2 Table shows following parameters . Column 1: galaxy name; Column 2: H I extent (R_{HI}), Column 3: average inclination angle (*i*); Column 4: computed values of $h_z \tan(i)$; Column 5: resolution beam size in pc units (Walter et al. (2008)); Column 6: Chosen ΔR . References are already mentioned in table 5.1 121

